

X-ray Structure and Electrochemical Properties of Ferrocene-Substituted Metalloporphyrins

Jinkwon Kim,^{*} Seog Woo Rhee,[†] Yong Hwan Na, Key Pyoung Lee, Youngkyu Do,^{†,*} and Sae Chae Jeoung[‡]

Department of Chemistry and RRC/NMR Kongju National University, Kongju 314-701, Korea

[†]*Department of Chemistry, School of Molecular Science-BK21 and Center for Molecular Design and Synthesis
Korea Advanced Institute of Science and Technology, Taejon 305-701, Korea*

[‡]*Laser Metrology Group, Korea Research Institute of Standards and Science, P.O. Box 102, Taejon 305-600, Korea
Received June 4, 2001*

Transition metal complexes of novel mono- and di-ferrocene-substituted porphyrins have been synthesized and characterized by structural and electrochemical methods. The X-ray structures of Mn(FPTTP)Cl and Mn(DFTTP)Cl showed the distorted square pyramidal coordination geometry with *syn* configuration of chloride and ferrocenyl substituents. The electrochemistry of ferrocene-substituted porphyrins and their metal complexes has been determined to elucidate the π -conjugation effect of the porphyrin ring. The ferrocenyl group of H₂FPTTP underwent a reversible one-electron transfer process at 0.30 V, indicating the good electron donating effect of the porphyrin ring to the ferrocene substituent. The redox potential of the ferrocenyl subunit and porphyrin ring was affected by the central metal ions of the metalloporphyrins, that is, Zn(II) and Ni(II) made the oxidation of ferrocene much easier and Mn(III) made it harder. The ferrocene subunits of H₂DFTTP interacted electrochemically with each other with peak splitting of 0.21 V. The strength of the electrochemical interactions between the two ferrocenyl substituents can be controlled by central metal ions of metalloporphyrins.

Keywords : Porphyrins, Ferrocene, Electrochemical, π -Conjugation.

Introduction

Many discrete molecules in which two redox active sites are linked by π -conjugation have been developed with great interests for applications in molecular electronic devices.^{1,2} In particular, ferrocene derivatives are the most frequently used molecules for this purpose. Conjugated systems containing two ferrocene units can be expected to show intramolecular and intermolecular interactions, so-called electrochemical communication, of the ferrocenyl groups.³ That is the reason why much effort has been made to develop the conjugated diferrocenyl derivatives. When one of the two ferrocenyl groups is oxidized to the monocation, the delocalization of the cationic charge between ferrocene and ferrocenium ion may occur to give a mixed valence state.⁴⁻⁶

Ferrocenes linked by olefin bridges show larger metal-metal interactions than those linked by analogues of saturated carbon. Recent studies identify a combination of factors that influence electrochemical interaction between connected ferrocene moieties, including the type of the connection,⁸ the length of the connector⁹ and the orientation of the two ferrocenes.¹⁰ For example, the series of polyene bridged bimetallic Fc(CH=CH)_nFc (*n* = 1-6, all *trans*) had been studied. The peak separations of 0.17, 0.13 and *ca.* 0.10 V were observed in dichloromethane for *n* = 1, 2, and 3 species, respectively, and peak separation was not resolved in the longer species.⁹

The combination of a porphyrin system and organometallic fragments within the same molecule may be interesting in terms of both intramolecular charge-transfer and catalytic properties.¹¹⁻²⁵ In particular, porphyrin-ferrocene conjugates have great potential in such areas as chemical sensors, porphyrin-assisted electron transfer, solar energy conversion, small molecule activation, and molecular devices. One can expect that the presence of a direct bond between the porphyrin and metallocene would lead to novel approaches in the application of porphyrins.

In the present study, we report the preparation and structures of transition metal complexes of mono- and di-ferrocenylporphyrin ligands and the effect of central metal ion on the electrochemical interactions among metal centers through extended π -conjugation of porphyrin ring.

Experimental Sections

Chemicals. All chemicals were of reagent grade, purchased from Aldrich Chemical Co., Fisher Chemical Co. or Sigma Chemical Co. and were used without further purification except as noted below. Solvents were purified according to standard methods.²⁶ All solvents were distilled from their sodium benzophenone ketyl solutions (toluene, tetrahydrofuran), from P₂O₅ (dichloromethane, chloroform and acetonitrile) or from CaH₂ (methanol) under a dinitrogen atmosphere.

Methods and Instruments. All manipulations of oxygen- and water-sensitive materials were performed either in a glove box or in Schlenk ware in an inert atmosphere.

^{*}To whom correspondence should be addressed. Tel: +82-41-850-8496; Fax: +82-41-850-8479; e-mail: jkim@kongju.ac.kr

Elemental analyses for C, H and N were performed by Fisons EA 1110 analyzer at the Energy & Environment Research Center of Korea Advanced Institute of Science and Technology. ^1H NMR spectra were obtained on a Bruker Spectrospin 400 spectrometer. In ^1H NMR spectra, chemical shifts (δ) were referenced against the residual signals of deuterated NMR solvents (7.24 for chloroform). UV/VIS spectra were recorded on a Shimadzu 3100s spectrometer. Electrochemical measurements were carried out on a Bio-Analytical Systems BAS-100W with Pt working electrode (1.6 mm diameter disk electrode), a Pt wire auxiliary electrode (5 cm length of 0.5 mm diameter wire), and a Ag/AgCl reference electrode with a vycor salt bridge. Cyclic voltammetry (CV) was performed with 1.0 mM solution of sample in dry CH_2Cl_2 containing 0.1 M of (*n*-Bu₄N)ClO₄ as supporting electrolyte with a scan rate 0.1 V min⁻¹ at room temperature. Under these condition ferrocene showed a reversible one-electron oxidation wave ($E_{1/2} = 0.37$ V). The solution was deaerated by bubbling dinitrogen gas, and during the acquisition dinitrogen was slowly flowed above the solution.

Synthesis. Tetra-*n*-butylammonium perchlorate (TBAP) was synthesized and purified by the procedure described in the literature²⁷ and was dried on P₂O₅ at 40 °C overnight before use. 5-ferrocenyl-15-phenyl-2,8,12,18-tetraethyl-3,7,13,17-tetramethylporphyrin (H₂FPTTP) and 5,15-diferrocenyl-2,8,12,18-tetraethyl-3,7,13,17-tetramethylporphyrin (H₂DFTTP) were synthesized and purified by the procedures reported previously.^{24,25}

5-Ferrocenyl-15-phenyl-2,8,12,18-tetraethyl-3,7,13,17-tetramethylporphyrinato metal complexes (M(FPTTP) (M = Mn(III)Cl, Ni(II) and Zn(II)). Porphyrin H₂FPTTP · 0.5C₆H₅Me (0.30 g, 0.38 mmol) was dissolved in dry CHCl₃ (200 mL). After the solution was deaerated by bubbling with dinitrogen for 30 min and refluxed for 15 min, 100 mL of a saturated solution of MnCl₂·4H₂O in methanol was added to the reaction flask *via* cannula for 30 min. The mixture was stirred and refluxed for 2 h under dinitrogen and then exposed to air and stirred for an additional 1 h at room temperature. The mixture was washed with 1 N HCl (1 × 200 mL) followed by washing with water and evaporation of solvent. By column chromatography on neutral Al₂O₃ (3 × 25 cm, CHCl₃) the unreacted free base porphyrin (H₂FPTTP) was removed effectively from the reaction mixture. Recrystallization from chloroform/*n*-pentane mixture at 0 °C gave deep green crystals of Mn(FPTTP)Cl · 0.5CHCl₃ (0.20 g, 58%). Anal. Calcd for Mn(FPTTP)Cl · 0.5CHCl₃ (C_{48.5}H_{48.5}N₄FeMnCl_{2.5}, MW; 886.864): C; 65.68, H; 5.51, N; 6.32. Found: C; 65.12, H; 5.77, N; 6.27. UV/VIS (CHCl₃) [λ_{max} , nm (log ϵ , M⁻¹ cm⁻¹)] 375 (4.61), 488 (4.60), 601 (3.86), 651 (3.75).

Ni(FPTTP) and Zn(FPTTP) were prepared by the same synthetic procedure. Ni(FPTTP): 95% yield. Anal. Calcd for Ni(FPTTP) · 0.5C₆H₅Me (C_{51.5}H₅₂N₄FeNi) (MW 841.19): C; 73.53, H; 6.23, N; 6.66. Found: C; 72.61, H; 6.38, N; 6.89. ^1H NMR (δ ppm, CDCl₃) 9.14 (s, 2H, *meso*-H), 8.40 (br, 1H, phenyl), 7.65 (br m, 4H, phenyl), 7.24 (m, 1.5H, phenyl of C₆H₅Me), 7.16 (m, 1H, phenyl of C₆H₅Me), 4.40 (s, 2H,

cyclopentadienyl), 4.34 (s, 2H, cyclopentadienyl), 3.73-3.53 (m, 8H, CH₂CH₃), 3.43 (s, 5H, cyclopentadienyl), 3.20 (s, 6H, CH₃), 2.35 (s, 1.5H, C₆H₅Me), 2.21 (s, 6H, CH₃), 1.59 (m, 12H, CH₂CH₃). UV/VIS (C₆H₅Me) [λ_{max} , nm (log ϵ , M⁻¹ cm⁻¹)] 426 (4.97), 564 (4.15), 604 (4.05). Zn(FPTTP): 77% yield. Anal. Calcd for Zn(FPTTP) (C₄₈H₄₈N₄FeZn, MW; 802.17): C; 71.87, H; 6.03, N; 6.98. Found: C; 70.93, H; 6.37, N; 6.67. ^1H NMR (δ ppm, CDCl₃) 9.81 (s, 2H, *meso*-H), 8.26 (d, 1H, phenyl), 7.75 (t, 3H, phenyl), 7.71 (d, 1H, phenyl), 4.52 (t, 2H, cyclopentadienyl), 4.50 (s, 2H, cyclopentadienyl), 3.85 (m, 8H, CH₂CH₃), 3.52 (s, 5H, cyclopentadienyl), 3.38 (s, 6H, CH₃), 2.35 (s, 6H, CH₃), 1.73 (t, 6H, CH₂CH₃), 1.68 (t, 6H, CH₂CH₃). UV/VIS (C₆H₅Me) [λ_{max} , nm (log ϵ , M⁻¹ cm⁻¹)] 428 (5.26), 572 (4.12), 616 (3.95).

5,15-Diferrocenyl-2,8,12,18-tetraethyl-3,7,13,17-tetramethylporphyrinato metal complexes (M(DFTTP) (M = Mn(III)Cl, Ni(II) and Zn(II)). Complexes were made by using 0.35 g (0.39 mmol) of porphyrin H₂DFTTP · 0.5C₆H₅Me with the same synthetic procedure for Mn(FPTTP)Cl. Mn(DFTTP)Cl: Recrystallization from chlorobenzene/*n*-pentane mixture at 0 °C gave deep green crystals (0.23 g, 60%). Anal. Calcd for Mn(DFTTP)Cl (C₅₂H₅₂N₄Fe₂MnCl, MW; 935.098): C; 66.79, H; 5.61, N; 5.99. Found: C; 65.29, H; 6.02, N; 5.73. UV/VIS (CHCl₃) [λ_{max} , nm (log ϵ , M⁻¹ cm⁻¹)] 366 (4.54), 418 (4.62), 494 (4.53), 698 (3.95). Ni(DFTTP): Recrystallization from chloroform-methanol mixture gave purple crystals (0.24 g, 68%). Anal. Calcd for Ni(DFTTP) (C₅₂H₅₂N₄Fe₂Ni, MW; 903.05): C; 69.16, H; 5.80, N; 6.20. Found: C; 70.8, H; 6.01, N; 6.48. ^1H NMR (δ ppm, CDCl₃) 8.83 (s, 2H, *meso*-H), 4.56 (s, 4H, cyclopentadienyl), 4.40 (s, 4H, cyclopentadienyl), 3.52 (m, 8H, CH₂CH₃), 3.22 (s, 10H, cyclopentadienyl), 3.16 (s, 12H, CH₃), 1.56 (m, 12H, CH₂CH₃). UV/VIS (C₆H₅Me) [λ_{max} , nm (log ϵ , M⁻¹ cm⁻¹)] 441 (4.47), 527 (4.15). Zn(DFTTP): Recrystallization from chloroform-methanol mixture gave purple crystals (0.32 g, 90%). Anal. Calcd for Zn(DFTTP) (C₅₂H₅₂N₄Fe₂Zn, MW; 910.10): C; 68.63, H; 5.76, N; 6.16. Found: C; 69.9, H; 6.01, N; 5.93. ^1H NMR (δ ppm, CDCl₃) 9.54 (s, 2H, *meso*-H), 4.62 (s, 4H, cyclopentadienyl), 4.54 (s, 4H, cyclopentadienyl), 3.79 (m, 8H, CH₂CH₃), 3.65 (s, 10H, cyclopentadienyl), 3.31 (s, 12H, CH₃), 1.66 (t, 12H, CH₂CH₃). UV/VIS (C₆H₅Me) [λ_{max} , nm (log ϵ , M⁻¹ cm⁻¹)] 468 (4.54), 617 (4.52), 577 (4.27).

X-ray structural determination. Mn(FPTTP)Cl · 0.5CHCl₃. The green colored single crystals of Mn(FPTTP)Cl · 0.5 CHCl₃ were obtained by slow cooling of chloroform/*n*-pentane solution at 0 °C. The single crystal with dimension 0.5 × 0.5 × 0.3 mm was mounted on a thin glass fiber at room temperature. Data collection was performed on an Enraf-Nonius CAD4 Diffractometer equipped with graphite-monochromated Mo K α ($\lambda = 0.71073$ Å) radiation. Accurate unit cell parameters and an orientation matrix were determined from a least-squares fit of 25 accurately centered reflections ($19.64^\circ < 2\theta < 28.11^\circ$). These dimensions and other parameters, including conditions of data collection, are summarized in Table 1. Data were collected at 293(2) K in the ω scan mode. Three intense reflections were monitored every 200 reflections to check stability. Of the 5836 unique

Table 1. Crystallographic Data for Mn(FPTTP)Cl·0.5CHCl₃ and Mn(DFTTP)Cl

	Mn(FPTTP)Cl·0.5CHCl ₃	Mn(DFTTP)Cl
empirical formula	C _{48.5} H _{48.5} N ₄ FeMnCl _{2.5}	C ₅₂ H ₅₂ N ₄ Fe ₂ MnCl
formula weight	886.83	935.07
crystal system	orthorhombic	monoclinic
space group	<i>F</i> 2 <i>dd</i> (No.43)	<i>P</i> 2 ₁ / <i>c</i> (No. 14)
<i>a</i> , Å	15.706(2)	13.198(2)
<i>b</i> , Å	24.807(2)	25.043(2)
<i>c</i> , Å	43.216(2)	14.238(2)
α , °	90	90
β , °	90	114.8(2)
γ , °	90	90
<i>V</i> , Å ³	16838(3)	4272.6(9)
<i>Z</i>	16	4
ρ_{calcd} , g cm ⁻³	1.400	1.454
$\lambda(\text{Mo}/\text{K}\alpha)$, Å	0.71073	0.71073
μ , mm ⁻¹	0.843	1.066
crystal size, mm	0.5 × 0.5 × 0.3	0.3 × 0.3 × 0.3
scan mode	ω	ω/θ
no. reflns total	5836	7497
no. data ($I > 2\sigma(I)$)	4515	4116
no. parms. refined	490	541
R_1 ($I > 2\sigma(I)$) ^a	0.0564	0.0468
wR_2 ($I > 2\sigma(I)$) ^b	0.1344	0.1078
<i>x</i>	0.0827	0.0568
<i>y</i>	35.6914	0.0000
GOF	1.088	1.230

^aStructure was refined in F_o^2 using all data; the value of R_1 is given for comparison with older refinements based on F_o with a typical threshold of $F_o > 4\sigma(F_o)$. $R_1 = \sum||F_o| - |F_c|| / \sum|F_o|$. ^b $wR_2 = [\sum[w(F_o^2 - F_c^2)^2 / \sum[w(F_o^2)^2]]^{1/2}$, where $w = 1/[\sigma^2(F_o^2) + (x \cdot P)^2 + y \cdot P]$, where $P = (F_o^2 + 2F_c^2)/3$.

reflections measured, 4515 were considered observed ($I_o > 2\sigma(I_o)$) and were used in subsequent structure analysis. Data were corrected for Lorentz and polarization effects. Semi-empirical absorption correction, using the ψ scan technique was applied. The SHELXS-86 program was utilized for the direct method. The structure refinements were performed with the SHELXL-93 program on F^2 data. Anisotropic thermal parameters for all non-hydrogen atoms were included in the refinements. All hydrogen atoms bonded to carbon atoms were included in calculated positions. This C-H bond distance was fixed and U values were assigned based approximately on the U value of the attached atom. Chlorine and carbon atoms of disordered solvent (chloroform) were refined with fixed site occupation factor of 0.5. The solvent hydrogen was included in located positions with $U = 0.08$ Å². A final difference Fourier map revealed several random features (< 0.284 eÅ⁻³). The full-matrix least-squares refinement finally converged with $R_1 = 0.0564$ (based on F) and $wR_2 = 0.1344$ (based on F^2) for observed reflections ($I_o > 2\sigma(I_o)$).

Mn(DFTTP)Cl. The green colored single crystals of Mn(DFTTP)Cl were obtained by slow cooling of chlorobenzene/*n*-pentane solution at 0 °C. The single crystal with

dimension $0.3 \times 0.3 \times 0.3$ mm was mounted on a thin glass fiber at room temperature. Data collection was performed on an Enraf-Nonius CAD4 Diffractometer equipped with graphite-monochromated Mo K α ($\lambda = 0.71073$ Å) radiation. Accurate unit cell parameters and an orientation matrix were determined from a least-squares fit of 25 accurately centered reflections ($20.00^\circ < 2\theta < 30.20^\circ$). These dimensions and other parameters, including conditions of data collection, are summarized in Table 1. Data were collected at 293 K in the ω/θ scan mode. Three intense reflections were monitored every 200 reflections to check stability. Of the 7497 unique reflections measured, 4116 were considered observed ($I_o > 2\sigma(I_o)$) and were used in subsequent structure analysis. Data were corrected for Lorentz and polarization effects. Semi-empirical absorption correction, using the ψ scan technique, was applied. The SHELXS-86 program was utilized for the direct method. The structure refinements were performed with the SHELXL-93 program on F^2 data. Anisotropic thermal parameters for all non-hydrogen atoms were included in the refinements. All hydrogen atoms bonded to carbon atoms were included in calculated positions. This C-H bond distance was fixed, and U values were assigned based approximately on the U value of the attached atom. A final difference Fourier map revealed several random features (< 0.549 eÅ⁻³). The full-matrix least-squares refinement finally converged with $R_1 = 0.0468$ (based on F) and $wR_2 = 0.1078$ (based on F^2) for observed reflections ($I_o > 2\sigma(I_o)$).

Results and Discussion

Structural description of Mn(FPTTP)Cl and Mn(DFTTP)Cl. The X-ray structures of Mn(FPTTP)Cl and Mn(DFTTP)Cl show the distorted square pyramidal geometry of a five coordinate system as shown in Figure 1 and Figure 2. This coordination geometry is quite common in porphyrinato-manganese(III) halide systems.²⁸

In the free base porphyrin H₂FPTTP, steric bulkness of β -pyrrolyl methyl groups not only prevents the ferrocenyl group from rotating around the *meso* carbon but also results in the distortion of the porphyrin ring.²⁴ The porphyrin skeleton of Mn(FPTTP)Cl is more distorted with ruffle deformation than the porphyrin skeleton of free base H₂FPTTP, because metal complexation causes contraction of the porphyrin ring, thus leading to increase steric hindrance between the ferrocenyl group and the β -pyrrolyl methyl groups. Deviations of *meso*-positioned carbon atoms and Mn atom from the mean plane of nitrogen atoms are listed in Table 2.

The C5-C_{Fe} distance of 1.488 Å is slightly shorter than 1.505 Å of free base.²⁴ The C5-C α distances (1.401 and 1.413 Å) and the C15-C α bond distances (1.389 and 1.405 Å) are similar to each other. The angles of C α -C5-C α (119.9°) and C α -C15-C α (122.1°) are slightly reduced compared with those of H₂FPTTP.²⁴ The C α -C5-C_{Fe} angles of 115.6° and 124.0° indicate that the Cp ring is tilted to one side to reduce the steric strains in the crystal. The average distance of shorter N...N is 2.723 Å and the longer is 2.858

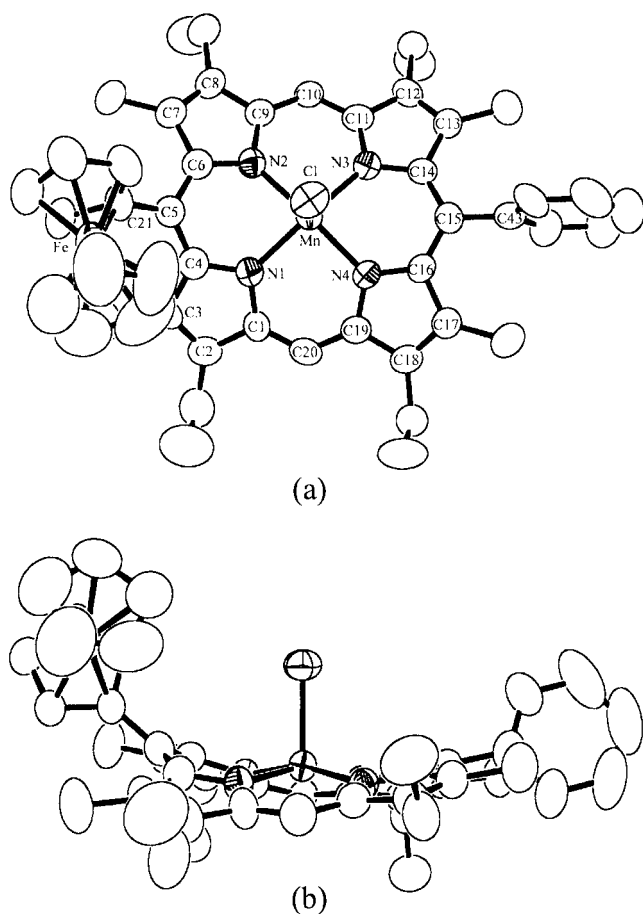


Figure 1. Molecular structure of porphyrin Mn(FPTTP)Cl. (a) top view and (b) side view. Ellipsoids are drawn for 50% probability, and hydrogen atoms have been omitted for clarity.

Å, resulting in approximately square planar geometry. A difference of 0.135 Å between two types of N···N distances in Mn(FPTTP)Cl is smaller than that (0.436 Å) of H₂FPTTP, due to coordination of manganese(III) ion. The average Mn-N distance is 2.001 Å, and Mn-Cl is 2.358 Å, similar to the values of Mn(TPP)Cl reported in the literature.²⁹ Mn-Ct distance of 0.332 Å, the displacement of the Mn(III) ion from the basal plane defined by the four nitrogen atoms in porphyrin macrocycle, is slightly longer than Mn-Ct distance of 0.27 Å of Mn(TPP)Cl.²⁹ The Mn-Cl distance of 2.358 Å suggests an appreciable amount of covalent character of the bonding. The selected bond lengths and angles are listed in Table 3.

In the case of porphyrins with unsymmetrical substituents at 5 and 15 positions, *syn*- and *anti*-atropisomers are expected to form. However, it has been elucidated that two ferrocenyl groups of H₂DFTTP prefer to be aligned in a *syn*-axial mode to reduce large steric repulsion between the ferrocenyl moiety and the adjacent methyl side chains. Furthermore, such a large steric repulsion leads to severe ruffle deformation.²⁵ The structure of Mn(DFTTP)Cl is also more distorted than that of H₂DFTTP, due to the same reason in the complex Mn(FPTTP)Cl. The C-C distances (C5-C21; 1.477 and C15-C31; 1.485 Å) between the Cp ring and

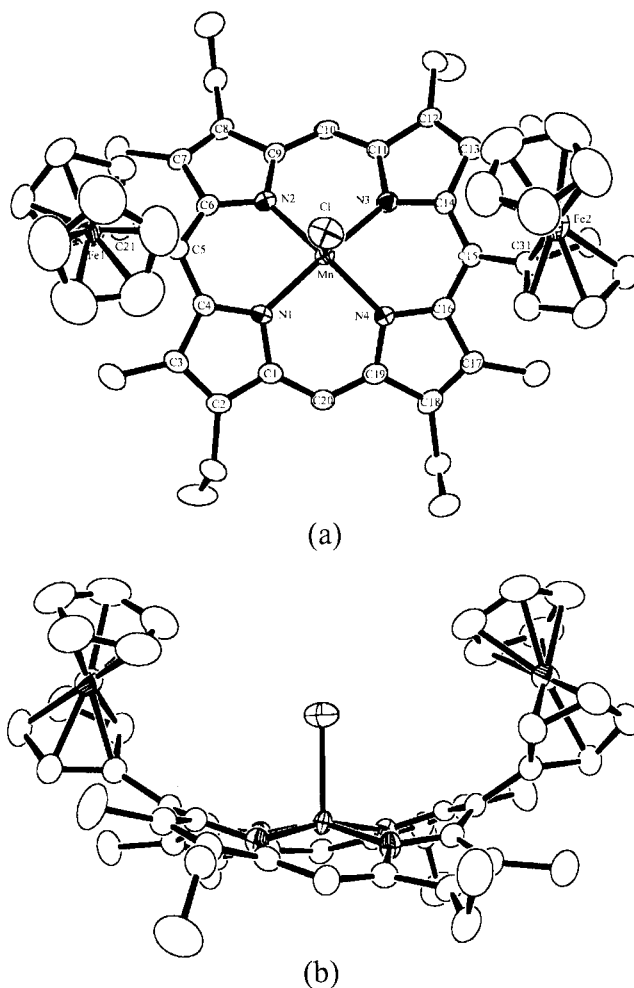


Figure 2. Molecular structure of porphyrin Mn(DFTTP)Cl. (a) top view and (b) side view. Ellipsoids are drawn for 50% probability, and hydrogen atoms have been omitted for clarity.

Table 2. Deviations (Å) of C_{meso} and Mn from mean plane of nitrogen atoms

	1	2	Mn(FPTTP)Cl	Mn(DFTTP)Cl
C5	0.281	0.535	0.657	0.727
C10	-0.225	-0.610	-0.566	-0.576
C15	0.092	0.579	0.444	0.659
C20	-0.163	-0.519	-0.550	-0.620
Mn			0.332	0.327

meso-carbon are similar to those of free base porphyrin (1.498 Å and 1.488 Å), implying a very weak conjugation between the porphyrin ring and the ferrocenyl group. The average of the C_{meso}-C_α distances is 1.418 Å and the average of the C_α-C_{meso}-C_α angles is 119.5°. The Cp rings are also tilted to one side of porphyrin plane. There are two kinds of N···N distances; one shorter (average 2.688 Å) and the other longer (average 2.848 Å) in the N₄ tetragonal core. The difference of 0.160 Å between the two types of N···N distances in Mn(DFTTP)Cl is slightly smaller than 0.371 Å of H₂DFTTP. The average Mn-N distance is 1.986 Å, the

Table 3. Selected bond distances (Å) and bond angles (°) for Mn(FPTTP)Cl·0.5CHCl₃

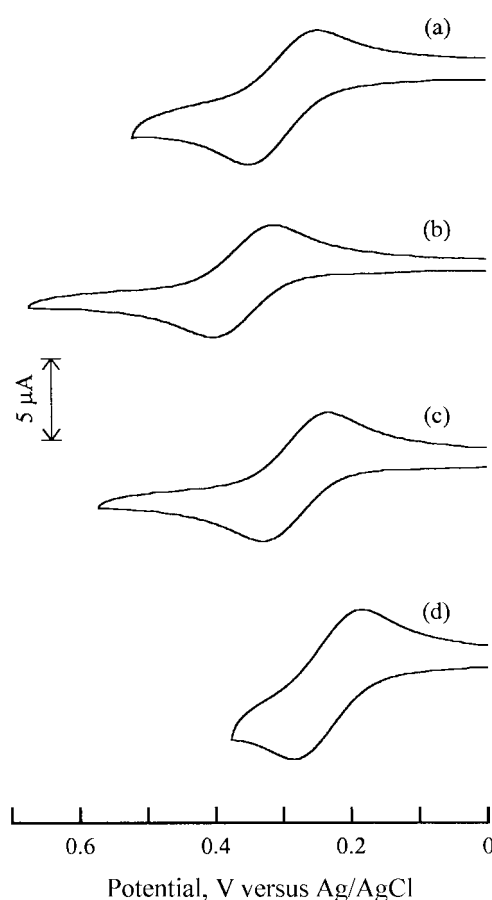
distances (Å)			
Mn --- N1	2.010(5)	Mn --- N2	1.985(6)
Mn --- N3	2.003(5)	Mn --- N4	2.006(5)
Mn --- Cl1	2.358(2)	C5 --- C21	1.488(8)
C15 --- C43	1.478(8)		
angles (°)			
N1 ... N2	2.709	N3 ... N4	2.737
N1 ... N4	2.866	N2 ... N3	2.849
angles (°)			
N1 - Mn - N2	85.4(2)	N1 - Mn - N3	159.1(2)
N1 - Mn - N4	91.1(2)	N2 - Mn - N3	91.2(2)
N2 - Mn - N4	162.8(2)	N3 - Mn - N4	86.1(2)
N1 - Mn - Cl1	100.0(2)	N2 - Mn - Cl1	97.9(2)
N3 - Mn - Cl1	101.0(2)	N4 - Mn - Cl1	99.3(2)
C4 - C5 - C6	119.9(7)	C4 - C5 - C21	124.0(7)
C6 - C5 - C21	115.6(6)	C14 - C15 - C16	122.1(6)
C14 - C15 - C43	118.0(6)	C16 - C15 - C43	119.6(6)

Mn-Cl distance is 2.363 Å, and the distance of Ct-Mn is 0.329 Å. The selected bond lengths and angles are listed in Table 4.

Regarding the location of the chloride ion, two stereoisomers are possible in both Mn(FPTTP)Cl and Mn(DFTTP)Cl. The axial chloride ion is potentially located on the same side of ferrocene with *syn* configuration or the opposite side of ferrocene with *anti* configuration. However, both Mn(FPTTP)Cl and Mn(DFTTP)Cl have been isolated with only *syn* configuration. Notably, a single isomer was obtained with the sterically less preferred form in both molecules. Mn(II) ion was coordinated by porphyrin under unaerobic reaction conditions, forming a square planar complex. Then, it was oxidized into Mn(III) ion by dioxygen of air under acidic media, and chloride ion was incorporated into the axial

Table 4. Selected bond distances (Å) and bond angles (°) for Mn(DFTTP)Cl

distances (Å)			
Mn --- N1	1.998(5)	Mn --- N2	1.976(3)
Mn --- N3	1.999(5)	Mn --- N4	1.972(3)
Mn --- Cl	2.363(1)	C5 --- C21	1.477(5)
C15 --- C31	1.485(5)		
angles (°)			
N1 ... N2	2.682	N1 ... N4	2.848
N2 ... N3	2.848	N3 ... N4	2.703
angles (°)			
N1 - Mn - N2	84.9(2)	N1 - Mn - N3	163.8(1)
N1 - Mn - N4	91.6(2)	N2 - Mn - N3	91.5(2)
N2 - Mn - N4	158.1(1)	N3 - Mn - N4	85.8(2)
N4 - Mn - Cl	100.2(1)	N2 - Mn - Cl	101.7(1)
N1 - Mn - Cl	97.9(1)	N3 - Mn - Cl	98.3(1)
C4 - C5 - C6	119.5(4)	C4 - C5 - C21	128.4(4)
C6 - C5 - C21	112.0(4)	C14 - C15 - C16	119.5(4)
C14 - C15 - C31	127.7(4)	C16 - C15 - C31	112.6(4)

**Figure 3.** Cyclic voltammograms of (a) free base porphyrin H₂FPTTP (b) Mn(FPTTP)Cl (c) NiFPTTP, and (d) ZnFPTTP recorded at a platinum electrode in dichloromethane solutions (1 mM). Scan rate is 0.1 V min⁻¹.

positions of complex to compensate for the positive charge. Stereochemistry seems to be determined at this stage. Such stereoselectivity has been rarely observed in the metalloporphyrin chemistry.³⁰ Steric bulkness of ferrocenyl groups at *meso*-positions may play a role in determining a stereoselective isomer.

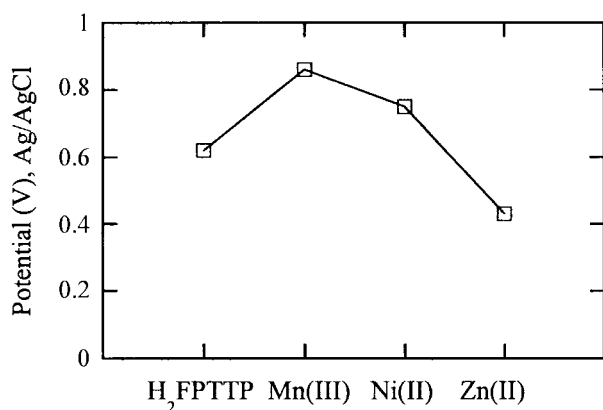
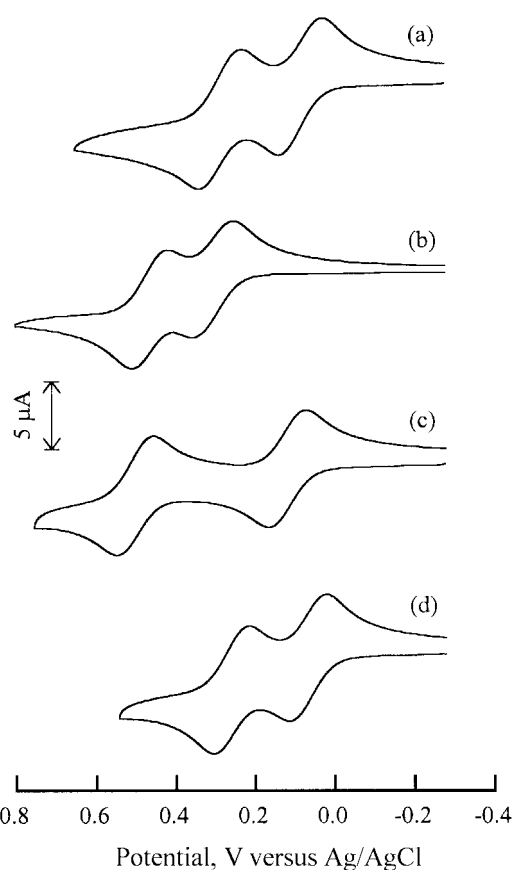
Electrochemistry of porphyrins. Electrochemistry provides some information on the π -conjugated porphyrin systems. The cyclic voltammograms of free base H₂FPTTP and its metal complexes are displayed in Figure 3, and the half-wave potentials of free base porphyrins and their transition metal complexes in dichloromethane solution are summarized in Table 5. The ferrocenyl group of H₂FPTTP undergoes reversible one-electron transfer process at $E_{1/2} = 0.30$ V. Such a value indicates that the ferrocenyl group is more susceptible to oxidation than the molecular ferrocene. This easier ferrocenyl oxidation might be considered a consequence of electron releasing ability of the porphyrin ring. Because electron density might be transferred from porphyrin macrocycle to ferrocene through π -conjugation, ferrocene can be oxidized more easily. Moreover, the monocation formed by oxidation is stabilized by delocalization of the positive charge over the porphyrin ring system.

Table 5. Half-wave potentials (V versus Ag/AgCl), anodic-cathodic peak potential separations (ΔE_p , V) and peak separations between two redox waves ($\Delta E_{1/2}$, V) of ferrocene moieties in porphyrins

	Fc ⁰ /Fc ⁺ (ΔE_p)	Fc ⁺ /Fc ²⁺ (ΔE_p)	$\Delta E_{1/2}$
H ₂ FPTTP	0.30 (0.10)		
Mn(FPTTP)Cl	0.36 (0.09)		
NiFPTTP	0.28 (0.10)		
ZnFPTTP	0.23 (0.10)		
H ₂ DFTTP	0.08 (0.10)	0.29 (0.10)	0.21
Mn(DFTTP)Cl	0.30 (0.11)	0.47 (0.09)	0.17
NiDFTTP	0.11 (0.10)	0.50 (0.09)	0.39
ZnDFTTP	0.07 (0.09)	0.27 (0.09)	0.20
FcH	0.37		

The redox potentials of ferrocene moiety are also affected by the central metal ion in metalloporphyrins. The oxidation potential of the ferrocene moiety of NiFPTTP shifts toward the positive direction compared with that of ZnFPTTP, which can be explained by the inductive effects of the central metals. Ni(II) ion has an electronegativity of 1.8, while Zn(II) has the value of 1.5. The electron density of the porphyrin ring is increased by π -back donation from metal to ligand. Zn(II) releases more electron density than Ni(II) to the porphyrin ring, thus the ferrocene of ZnFPTTP can be oxidized more easily than Ni(II). However, in the case of Mn(FPTTP)Cl, the higher oxidation state of Mn(III) reduces the electron releasing ability of the porphyrin ring to ferrocene, making ferrocene oxidation more difficult. In fact, the oxidation potential of ferrocenyl moiety of Mn(FPTTP)Cl shifts to a much more positive direction than H₂FPTTP. Electrochemical analyses show that the oxidation of the ferrocene subunit is strongly affected by the porphyrin ring as well as the central metal through extended π -conjugation.

The oxidation of porphyrin ring is also affected by the central metal. The half-wave potentials for the ring oxidation of free base porphyrin H₂FPTTP and its metal complexes are

**Figure 4.** Half-wave potentials for the oxidation of porphyrin ring in free base porphyrin H₂FPTTP and its metal complexes.**Figure 5.** Cyclic voltammograms of (a) free base porphyrin H₂DFTTP (b) Mn(DFTTP)Cl (c) NiDFTTP, and (d) ZnDFTTP recorded at a platinum electrode in dichloromethane solutions (1 mM). Scan rate is 0.1 V min⁻¹.

shown in Figure 4. The inductive effects of the central metals over the conjugative effects are of greater importance. The macrocycle ring containing more electron rich metal ion is oxidized more easily.

The cyclic voltammetric responses of H₂DFTTP and its metal complexes in dichloromethane solution are shown in Table 5 and Figure 5. The ferrocenyl groups of H₂DFTTP are more easily oxidized by two reversible one-electron processes than molecular ferrocene, revealing that the positive charges developed in monocation and dication are stabilized through an extended π -system and two ferrocene subunits interact with each other strongly. This strong coupling appears to be the result of the extensive mixing of both ferrocenyl molecular orbital systems with that of the porphyrin π -system. Metallation of ferrocenyl porphyrins also affects the oxidation potentials of the ferrocenyl groups, and the tendency of such effects is similar to those observed in the monoferrocenyl porphyrin H₂FPTTP. The largest separation of the oxidation potentials for the two ferrocenes observed in NiDFTTP indicates presumably that the effective overlap of t_{2g} orbitals of Ni(II) with π -orbitals of porphyrin ligand plays a key role in increasing electronic communication. Such an unusually strong electrochemical communication may be useful for the development of elec-

tronic devices.

Acknowledgment. This work was supported by the Korea Research Foundation (1999-015-DP0181).

Supplementary Material. X-ray crystallographic data for Mn(FPTTP)Cl·0.5CHCl₃ and Mn(DFTTP)Cl are available from the corresponding author upon request.

References

1. *Molecular Electronics*; Jortner, J., Ratner M., Eds.; IUPAC, Blackwell, 1997.
 2. (a) Fox, M. A. *Acc. Chem. Res.* **1999**, *32*, 201. (b) Metzger, R. M.; Panneta, C. A. *New J. Chem.* **1991**, *15*, 209.
 3. Barlow, S.; O'Hare, D. *Chem. Rev.* **1997**, *97*, 637.
 4. Kramer, J. A.; Hendrickson, D. N. *Inorg. Chem.* **1980**, *19*, 3330.
 5. Dong, T.-Y.; Hendrickson, D. N.; Iwai, K.; Cohn, M. J.; Geib, S. J.; Rheingold, A. L.; Sano, H.; Motoyama, I.; Nakashima, S. *J. Am. Chem. Soc.* **1985**, *107*, 7996.
 6. Barlow, S.; Murphy, V. J.; Evans, J. S. O.; O'Hare, D. *Organomet.* **1995**, *14*, 3461.
 7. Morrison, W. H.; Krogsrud, S.; Hendrickson, D. N. *Inorg. Chem.* **1973**, *12*, 1998.
 8. Tolbert, L. M.; Zhao, X.; Ding, Y.; Bottomley, L. A. *J. Am. Chem. Soc.* **1995**, *117*, 12891.
 9. Ribou, A.-C.; Launay, J.-P.; Sachtleben, A. L.; Li, H.; Spangler, C. W. *Inorg. Chem.* **1996**, *35*, 3735.
 10. Patoux, C.; Coudret, C.; Launay, J.-P.; Joachim, C.; Gourdon, A. *Inorg. Chem.* **1996**, *36*, 5037.
 11. Wollmann, R. G.; Hendrickson, D. N. *Inorg. Chem.* **1977**, *16*, 3079.
 12. Hisatome, M.; Takano, S.; Yamakawa, K. *Tetrahedron Lett.* **1985**, *26*, 2347.
 13. Schmidt, E. S.; Calderwood, T. S.; Bruice, T. C. *Inorg. Chem.* **1986**, *25*, 3718.
 14. Beer, P. D.; Kurek, S. S. *J. Organomet. Chem.* **1987**, *336*, 17; **1989**, *366*, 6.
 15. Giasson, R.; Lee, E. J.; Zhao, X.; Wrighton, M. S. *J. Phys. Chem.* **1993**, *97*, 2596.
 16. Loim, N. M.; Grishko, E. V.; Pyshnograeva, N. I.; Vorontsov, E. V.; Sokolov, V. I. *Russ. Chem. Bull.* **1994**, *43*, 871.
 17. Loim, N. M.; Kondratenko, M. A.; Grishko, E. V.; Sokolov, V. I. *Russ. Chem. Bull.* **1994**, *43*, 905.
 18. Sokolov, V. I. *J. Organomet. Chem.* **1995**, *500*, 299.
 19. Loim, N. M.; Abramova, N. V.; Sokolov, V. I. *Medeleev Commun.* **1996**, 46.
 20. Beer, P. D.; Drew, M. G. B.; Jagessar, R. *J. Chem. Soc. Dalton Trans.* **1997**, 881.
 21. Burrell, A. K.; Campbell, W. M.; Officer, D. L. *Tetrahedron Lett.* **1997**, *38*, 1249.
 22. Burrell, A. K.; Campbell, W. M.; Officer, D. L.; Scott, S. M.; Gordon, K. C.; McDonald, M. R. *J. Chem. Soc. Dalton Trans.* **1999**, 3349.
 23. Boyd, P. D. W.; Burrell, A. K.; Campbell, W. M.; Cocks, P. A.; Gordon, K. C.; Jameson, G. B.; Officer, D. L.; Zhao, Z. *Chem. Commun.* **1999**, 637.
 24. Rhee, S. W.; Park, B. B.; Do, Y.; Kim, J. *Polyhedron* **2000**, *19*, 1961.
 25. Rhee, S. W.; Na, Y. H.; Do, Y.; Kim, J. *Inorg. Chim. Acta* **2000**, *309*, 49.
 26. Perrin, D. D.; Armarego, W. L. F. *Purification of Laboratory Chemicals*; Pergamon Press: New York, 1988.
 27. Sawyer, D. T.; Sobkowiak, A.; Roberts, J. L., Jr. *Electrochemistry for Chemists*; John Wiley & Sons: New York, 1995; p 336.
 28. *The Porphyrins*; Dolphin, D., Ed.; Academic Press: New York, 1978; Vol. 3, p 463.
 29. Tulinsky, A.; Chen, B. M. L. *J. Am. Chem. Soc.* **1977**, *99*, 3647.
 30. Clement, T. E.; Nurco, D. J.; Smith, K. M. *Inorg. Chem.* **1998**, *37*, 1150.
-